

From Self-Assembled Microspheres to Self-Templated Nanotubes: Morphologies and Properties of Sulfur-Bridged Fluoranthene-Based Organic Materials

Xiao-Liang Fang, Shun-Liu Deng, Jing Wang, Xiao-Feng Wang, Cheng Chen, Yue Li, Su-Yuan Xie,* Rong-Bin Huang, and Lan-Sun Zheng

State Key Laboratory for Physical Chemistry of Solid Surfaces and Department of Chemistry, College of Chemistry and Chemical Engineering, Xiamen University, Xiamen 361005, P.R. China

Received July 3, 2009. Revised Manuscript Received November 2, 2009

The inability to controllably synthesize organic nanomaterials with desired morphologies and properties is a major barrier that prevents the scientific development of organic nanomaterials. A controllable method by means of adjusting the solubility of organic reactant has now been applied to construct sulfur-bridged fluoranthene-based materials with desired spherical or tubular morphologies, based on the Williamson type of reaction starting from perchlorinated fluoranthene and disodium salt of 2,5-dimercapto-1,3,4-thiadiazole. A disubstituted fluoranthene derivative is proved as the basic building block for the organic materials by the data of mass spectrometry, X-ray photoelectron spectroscopy, as well as crystallography. Through quenching the intermediates toward the fluoranthene-based microspheres or nanotubes, the routes of self-assembly via a vesicle pathway and self-template from perchlorinated fluoranthene rods are proposed for the growth of the microspheres and the nanotubes, respectively. The proposed routes can be extended for synthesis of other aromatic molecular materials with controllable morphologies. On the basis of the reaction with thiol groups retained on the surface of the as-synthesized materials, functional groups or noble metal nanoparticles have been facilely linked to the fluoranthene-based materials for potential applications. Morphology-dependent properties of the fluoranthene-based materials have been demonstrated, on the basis of the experimental evidence about strong near-infrared absorption exhibiting in the microspheres but lacking in the nanotubes.

1. Introduction

Many properties of materials are well-known to be morphology-dependent in nanoscale.¹ For example, catalytic effects of metal nano- or microparticles considerably rely on their polyhedral shape;² optical absorption spectra of organic dyes depend on their morphologies as well as sizes,³ and resonances in Raman scattering and fluorescence emission from nanoparticles are also morphology-dependent.⁴ Such a relationship between properties and morphologies stimulates scientists to controllably assemble a wide range of materials with different shapes or sizes in nano- or micrometer scale.

In the literature, a variety of small-sized morphologies such as spheres, tubes, wires, rods, and polyhedrons have been reported.⁵ Among them, inorganic materials including metals and their oxides (or sulfides) overwhelmingly dominate in this research field.⁶ In contrast, size- or morphology-controllable syntheses for traditional organic nanomaterials are apparently insufficient, which prevents the scientific development of organic nanomaterials even though they have shown promising chemical and optical properties.^{7–9} The methods for the synthesis of organic nanomaterials include reprecipitation,¹⁰ self-assembly,¹¹

*Corresponding author. Telephone: 86-592-2185191. Fax: 86-592-2183047. E-mail: syxie@xmu.edu.cn.

- (1) (a) El-Sayed, M. A. *Acc. Chem. Res.* **2004**, *37*, 326–333. (b) Burda, C.; Chen, X. B.; Narayanan, R.; El-Sayed, M. A. *Chem. Rev.* **2005**, *105*, 1025–1102.
(2) (a) Narayanan, R.; El-Sayed, M. A. *Nano Lett.* **2004**, *4*, 1343–1348. (b) Chen, J. Y.; Lim, B. K.; Lee, E. P.; Xia, Y. N. *Nano Today* **2009**, *4*, 81–95. (c) Tian, N.; Zhou, Z. Y.; Sun, S. G.; Ding, Y.; Wang, Z. L. *Science* **2007**, *316*, 732–735. (d) Tsung, C. K.; Kuhn, J. N.; Huang, W. Y.; Aliaga, C.; Hung, L. I.; Somorjai, G. A.; Yang, P. D. *J. Am. Chem. Soc.* **2009**, *131*, 5816–5822.
(3) (a) Kang, L. T.; Wang, Z. C.; Cao, Z. W.; Ma, Y.; Fu, H. B.; Yao, J. N. *J. Am. Chem. Soc.* **2007**, *129*, 7305–7312. (b) Balakrishnan, K.; Datar, A.; Naddo, T.; Huang, J. L.; Oitker, R.; Yen, M.; Zhao, J. C.; Zang, L. *J. Am. Chem. Soc.* **2006**, *128*, 7390–7398.
(4) (a) Eustis, S.; El-Sayed, M. A. *Chem. Soc. Rev.* **2006**, *35*, 209–217. (b) Zhang, J. T.; Li, X. L.; Sun, X. M.; Li, Y. D. *J. Phys. Chem. B* **2005**, *109*, 12544–12548.

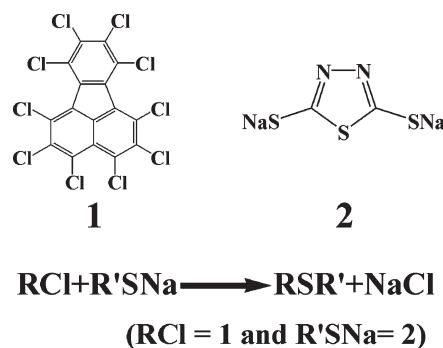
- (5) (a) Bong, D. T.; Clark, T. D.; Granja, J. R.; Ghadiri, M. R. *Angew. Chem., Int. Ed.* **2001**, *40*, 988–1011. (b) Xia, Y. N.; Yang, P. D.; Sun, Y. G.; Wu, Y. Y.; Mayers, B.; Gates, B.; Yin, Y. D.; Kim, F.; Yan, H. Q. *Adv. Mater.* **2003**, *15*, 353–389. (c) Xia, Y. N.; Xiong, Y. J.; Lim, B.; Skrabalak, S. E. *Angew. Chem., Int. Ed.* **2008**, *48*, 60–103.
(6) (a) Dai, Z. R.; Pan, Z. W.; Wang, Z. L. *Adv. Funct. Mater.* **2003**, *13*, 9–24. (b) Kwon, S. G.; Hyeon, T. *Acc. Chem. Res.* **2008**, *41*, 1696–1709.
(7) (a) Fu, H. B.; Xiao, D. B.; Yao, J. N.; Yang, G. Q. *Angew. Chem., Int. Ed.* **2003**, *42*, 2883–2886. (b) Tian, Z. Y.; Chen, Y.; Yang, W. S.; Yao, J. N.; Zhu, L. Y.; Shuai, Z. G. *Angew. Chem., Int. Ed.* **2004**, *43*, 4060–4063.
(8) Zhao, Y. S.; Fu, H. B.; Peng, A.; Ma, Y.; Xiao, D. B.; Yao, J. N. *Adv. Mater.* **2008**, *20*, 2859–2876.
(9) Jang, J.; Oh, J. H. *Adv. Mater.* **2003**, *15*, 977–980.
(10) Zhang, X. J.; Zhang, X. H.; Shi, W. S.; Meng, X. Y.; Lee, C. S.; Lee, S. T. *Angew. Chem., Int. Ed.* **2007**, *46*, 1525–1528.
(11) Zhao, Y. S.; Yang, W. S.; Xiao, D. B.; Sheng, X. H.; Yang, X.; Shuai, Z. Y.; Luo, Y.; Yao, J. N. *Chem. Mater.* **2005**, *17*, 6430–6435.

and soft/hard templates,¹² and the obtained organic nanostructures are usually constructed through noncovalent intermolecular interactions, such as hydrogen bonds, π - π interaction or van der Waals contacts.⁸ The difficulties in morphology-controllable assembly of organic materials are largely due to the common reason that the intermolecular interaction is typically too weak to regularly direct the random orientation of organic molecules for the formation of molecular materials with desired morphologies. Here we show that aromatic molecules can be constructed through thioether linker to form organic solid materials having uniform spherical or tubular morphologies. The morphologies are controllable through adjusting the solubility of organic reactant, involved in a traditional Williamson reaction starting from perchlorinated fluoranthene (**1**) and disodium salt of 2,5-dimercapto-1,3,4-thiadiazole (**2**) (Scheme 1). We paid special attentions to fluoranthene because it is a representative optical organic compound¹³ and a basic structural fragment with a pentagon and three hexagons for constructing three-dimensional molecular materials of fullerene.¹⁴ We have a long-standing interest in synthesis and properties of nonclassical fullerenes and their fragments, and in addition, their functionalization and application are investigated.¹⁵ Herein our experiments have demonstrated that, on the basis of morphologic and structural alteration, the near-infrared (NIR) absorption properties of the fluoranthene-based materials are morphology-dependent. The heretofore unknown routes accounting for the morphologic transformation of the organic solids from self-assembled microspheres to self-templated nanotubes have been investigated. In application aspects, the synthesized materials that display amphiphilic character because of the coexistence of hydrophilic and lipophilic units in their structures can be facilely functionalized with chemical groups or noble metal nanoparticles through the thiol groups retained on their surfaces to construct functional materials for fluorescent or catalytic applications.

2. Experimental Section

2.1. Chemicals. Metal sodium, ethanol, and toluene were purchased from Sinopharm Chemical Reagent Co. (Shanghai, China). 2,5-dimercapto-1,3,4-thiadiazole (DMTD) and 2-mercapto-5-methyl-1,3,4-thiadiazole were purchased from Alfa Aesar. Sodium sulfide nonahydrate ($\text{Na}_2\text{S}\cdot 9\text{H}_2\text{O}$) was purchased from the Xilong chemical Co. Ltd. (Guangzhou, China). All the

Scheme 1. Molecular Structures of Perchlorinated Fluoranthene (1) and the Disodium Salt of 2,5-Dimercapto-1,3,4-thiadiazole (2), and the Schematic Illustration of the Williamson Reaction



reagents were used without further purification. **1** was synthesized according to the method reported in the literature.¹⁶

2.2. Synthesis of the Ethanol Solution of 2. A mixture of metal sodium and ethanol was magnetically stirred at room temperature for 15 min, followed by adding DMTD into the solution. The solution was then stirred at room temperature for 2.5 h. The dosages of the reactants for producing the ethanol solution of **2** are as follows. (1) Involved in synthesis of the microspheres: metal sodium, 18 mg; ethanol, 5 mL; and DMTD, 60 mg. (2) Involved in the synthesis of the nanotubes: metal sodium, 9 mg; ethanol, 16 mL; and DMTD, 30 mg.

2.3. Synthesis of the Microspheres. Fifty-four milligrams of **1** was added to 10 mL of toluene. The reactant **1** was stirred until entirely dissolved, and then mixed with 5 mL of a pretreated ethanol solution of **2**. In a sealed 20 mL Teflon-lined autoclave, 15 mL of reactant mixture was heated at 180 °C for 24 h to afford the microsphere products.

2.4. Synthesis of the Nanotubes. Twenty-seven milligrams of **1** was added into 16 mL of an ethanol solution of **2**, and then 0.5 mL of toluene was added. The incompletely dissolved suspension mixture was put in an ultrasonic bath at room temperature for 1 min, and the suspension was added into a 20 mL Teflon-lined autoclave. The autoclave was sealed and maintained at 180 °C for 24 h to give the nanotube products.

2.5. Purification of the Products. The as-obtained products of microsphere or nanotube were centrifugated to afford crude solid products. The solids were cleaned and centrifugated in toluene, followed by washing with ethanol/deionized water (1:1) and then dispersing in pure ethanol. The operations of centrifuging, washing, and dispersing were repeated 10 times to give purified thiol-containing fluoranthene-based microspheres or nanotubes.

2.6. Characterization. Scanning electron microscopy (SEM) and transmission electron microscopy (TEM) images were taken on a LEO1530 microscope with a field-emission electron gun and a TECNAI F-30 high-resolution transmission electron microscope operating at 300 kV, respectively. The sample for SEM (or TEM) observations was prepared by dropping the ethanol suspension containing the uniformly dispersed products onto a silicon substrate (or a carbon-coated copper grid). The composition and crystal phase were checked by X-ray photoelectron spectroscopy (XPS, PHI QUANTUM2000 photoelectron spectrometer using a monochromatic magnesium X-ray source), energy-dispersive X-ray spectroscopy (EDX, equipped on TECNAI F-30 high-resolution transmission electron microscope), and X-ray diffraction (XRD, PANalytical X'pert pro, Cu KR radiation operating at 40 kV and 30 mA). The mass spectra were recorded in negative-ion mode on a Bruker-Esquiere HCT instrument interfaced by an atmospheric pressure

- (12) Lee, J. K.; Koh, W. K.; Chaeb, W. S.; Kim, Y. R. *Chem. Commun.* **2002**, 138–139.
- (13) Harvey, R. G. *Polycyclic Aromatic Hydrocarbons*; Wiley-VCH: Weinheim, Germany, 1997.
- (14) (a) Xie, S. Y.; Huang, R. B.; Chen, L. H.; Huang, W. J.; Zheng, L. S. *Chem. Commun.* **1998**, 2045–2046. (b) Tan, Y. Z.; Han, X.; Wu, X.; Meng, Y. Y.; Zhu, F.; Qian, Z. Z.; Liao, Z. J.; Chen, M. H.; Lu, X.; Xie, S. Y.; Huang, R. B.; Zheng, L. S. *J. Am. Chem. Soc.* **2008**, *130*, 15240–15241.
- (15) (a) Xie, S. Y.; Gao, F.; Lu, X.; Huang, R. B.; Wang, C. R.; Zhang, X.; Liu, M. L.; Deng, S. L.; Zheng, L. S. *Science* **2004**, *304*, 699. (b) Tan, Y. Z.; Liao, Z. J.; Qian, Z. Z.; Chen, R. T.; Wu, X.; Han, X.; Zhu, F.; Zhou, S. J.; Zheng, Z. P.; Lu, X.; Xie, S. Y.; Huang, R. B.; Zheng, L. S. *Nat. Mater.* **2008**, 790–795.
- (16) Ballester, M.; Molinet, C.; Castañer, J. *J. Am. Chem. Soc.* **1960**, *82*, 4254–4258.

chemical ionization (APCI) source. The Fourier transform infrared (FTIR) spectra were recorded in the range of $4000\text{--}400\text{ cm}^{-1}$ with a Nicolet AVATAR FT-IR 380 spectrometer, and the UV-vis-NIR spectra were recorded in the range of $300\text{--}2000\text{ nm}$ with a Varian Cary 5000 spectrometer. Crystal data collections were performed on an Oxford Diffraction Xcalibur 2 CCD diffractometer at 173 K. Absorption corrections were applied by using the multiscan program SADABS.¹⁷ The structures were solved by direct methods, and non-hydrogen atoms were refined anisotropically by least-squares on F^2 using the SHELXTL program.¹⁸ The hydrogen atoms of the organic group were generated geometrically ($C\text{--}H = 0.96\text{ \AA}$).

3. Results and Discussions

3.1. Morphologic Transformation of the Products. With the same dosages of reactants and the ratio of toluene/ethanol mixture as the synthesis of microspheres (see Experimental Section), the reaction involving **1** and **2** refluxing at $80\text{ }^\circ\text{C}$ in ambient air resulted in amorphous precipitation (see Figure S1 in the Supporting Information). These solid products are insoluble in any traditionally used polar or nonpolar organic solvents, such as toluene, benzene, chloroform, acetone, tetrahydrofuran, dimethylformamide, and chlorobenzene. In classical organic chemistry, such precipitation products should be avoided so as to circumvent the difficulties in structural identification of the organic solids. The resulting morphologies, however, can be dramatically uniform based on controlling the reaction conditions of the solvothermal process. Typically, the products can be morphology-controllable as microellipsoids, microspheres or nanotubes depending on adjustment of the solvent composition at the reaction temperature of $180\text{ }^\circ\text{C}$. As shown in Figure 1, the scanning electron microscopy (SEM) and transmission electron microscopy (TEM) images of the products clearly reveal the condition-dependent morphologies: (1) Ellipsoids dominate in the products if the volume ratio of toluene vs ethanol in the mixed solvent is 6:1 (Figure 1a). When the volume ratio of toluene vs ethanol is decreased to 2:1, the products are uniform sphere-shaped with diameter about $1\text{ }\mu\text{m}$ (Figure 1b). When the initial volume ratio is further decreased to 1:3, most of the products lose uniformity and give the mixture of spherical, tubular and shapeless particles (Figure 1c). (2) Reaction in 1:32 toluene:ethanol solvent results in nanotubes with length in micrometer scale, inner diameter in $200\text{--}400\text{ nm}$ and wall thickness in $30\text{--}40\text{ nm}$ (Figure 1d, e). Accordingly, morphologies of the products, such as the microspheres or the nanotubes to which we have paid special attention, are controllable depending on the component of solvent mixture as schematically depicted in Figure 1f.

3.2. Characterization of the Products. As expected, Fourier transform infrared (FTIR) spectral analyses reveal that the chemical compositions and vibrational

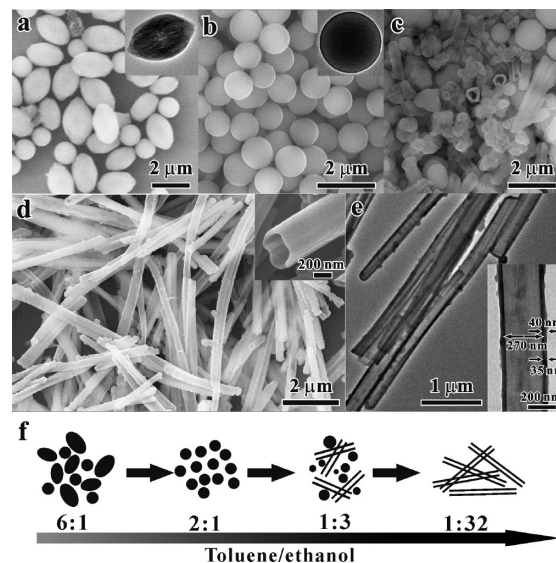


Figure 1. (a–e) SEM/TEM characterizations of the morphologies produced in different solvent mixture of toluene/ethanol with volume ratios of (a) 6:1, (b) 2:1, (c) 1:1, and (d, e) 1:32. The insets are the enlarged TEM/SEM images of corresponding products. (f) Schematic illustration for morphologies transformation of the products depending on volume ratio of toluene/ethanol.

characteristics of the products (the microspheres or the nanotubes) from the same kind of Williamson reaction are similar, regardless of their morphologies (see Figure S2 in the Supporting Information). The weak absorption around $3000\text{--}2900\text{ cm}^{-1}$ may be assigned to the stretching vibration of thiol group, while the absorption in the range of $1900\text{--}1200\text{ cm}^{-1}$ can be due to the conjugation $C=C$ vibration of aromatic moiety in the microspheres or the nanotubes. X-ray diffraction (XRD) spectra of the products reveal that both of the microspheres and the nanotubes are amorphous with a broadened peak around $20\text{--}30^\circ$ (2θ) (see Figure S3 in the Supporting Information). The components of C, N, O, S, and Cl in the purified products were established by X-ray photoelectron spectroscopy (XPS) (Figure 2), and the corresponding energy dispersive X-ray (EDX) spectra are shown in Figure S4 of the Supporting Information. The observed signals of oxygen are possibly due to the impurity in the products. The signals of Cl 2p located at around 200 eV can be assigned to the characteristic of Ar-Cl (Ar = aromatic group).¹⁹ The XPS also establishes the replacement of Na by H to form $-\text{SH}$ group after repeatedly washing of the products with deionized water (see Figure S5 and Table S1 in the Supporting Information). Such a $-\text{SH}$ group is useful for further surface functionalization with, for example, Rhodamine B and precious metals (vide infra). The four peaks of S 2p at $163.2, 164.0, 164.7,$ and 169.8 eV are the characteristics of Ar-S-, $-\text{SH}$, C-S-C (thiadiazole), and C-S(O)-, respectively.¹⁹ The sulfur content ratio in different groups is roughly 1.4:1:0.7 (for Ar-S-/C-S-C/ $-\text{SH}$), which can be calculated approximately from the peak area of

(17) Sheldrick, G. M. *SADABS 2.05*; University of Göttingen: Göttingen, Germany, 2001.

(18) Sheldrick, G. M. *SHELXTL*; Bruker Analytical Instrumentation: Madison, WI, 2000.

(19) Wagner, C. D.; Riggs, W. M.; Davis, L. E.; Moulder, J. F. *Handbook of X-Ray Photoelectron Spectroscopy*; Perkin-Elmer Corporation: Eden Prairie, MN, 1979.

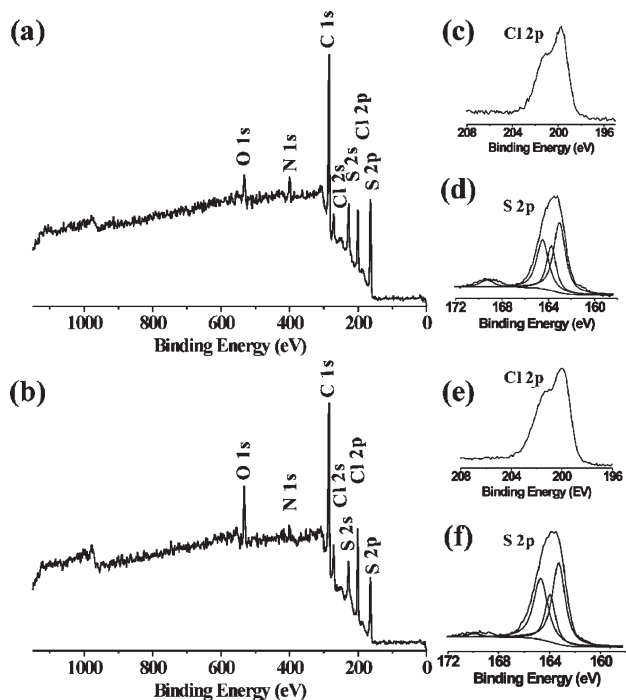


Figure 2. XPS spectra of the fluoranthene-based (a) microspheres and (b) nanotubes. (c–f) Enlarged XPS spectra of Cl 2p and S 2p electrons. The simulated XPS spectra of S 2p are amplified in Figure S6 in the Supporting Information.

Ar–S–, C–S–C, and –SH in the simulated XPS curves of the microspheres and the nanotubes (the insets in Figure 2 and Figure S6 in the Supporting Information). Considering the original sulfur content ratio of –SH vs C–S–C in the reactant 5-dimercapto-1,3,4-thiadiazole is 2:1, it is concluded that about one-third of thiol groups of the reactant **2** are retained to give the resultant thiol-containing fluoranthene-based materials.

3.3. Regioselective Reaction Involving 1 with 2. The Williamson reaction in solution has been known for almost 150 years and represents one of the conventional methods for constructing polymers linked with ether or thioether. We use this kind of reaction for the morphology-controllable synthesis of organic materials starting from **1** and **2** (Scheme 1). In principle, all 10 chlorines in **1** can potentially react with **2** to form highly substituted fluoranthene. As mentioned above, however, both the XPS and the EDX analyses have established that chlorines in **1** are partially replaced by **2**. To verify the most possible sites for bridging **1** with **2**, we conducted an otherwise-the-same reaction starting from an altered reactant of 2-mercapto-5-methyl-1, 3, 4-thiadiazole (**3**) (in replacement of **2**). In the hydrothermal conditions similar to the synthesis of the microspheres, the main products were characterized by mass spectra as tetra-substituted derivatives of **3**. Reaction at room temperature, however, produced a number of compounds with different number of substituted groups ($n = 1–4$) bonding to fluoranthene, as revealed in the mass spectra (Figure 3a, and the enlarged mass spectra shown in Figure S7 of the Supporting Information). To characterize the most reactive C–Cl sites of **1** and the structures of the products, we isolated individual compound from the

products by chromatographic method and obtained two types of single-crystals of mono- and trisubstituted products (**4** and **5**) for X-ray diffraction identification.^{20,21} As shown in Figure 3b, the crystallographic determinations of corresponding structures disclose that the first two reactive sites are the 5,10-chlorine positions next to the five-membered-ring. The second reactive chlorines are located at 7,8-positions according to the identified three-substituted structure (Figure 3c) as well as our previously reported reactions and structures about perchlorinated fluoranthene.²² Therefore, the regioselective reaction for the tetra-substitution involving **1** with **3** (or **2**) is almost certainly conducted at the 5, 7, 8, 10-chlorine (Figure 3d).

3.4. Building Blocks for the Fluoranthene-Based Materials. To further investigate the reactions and the resultant structures, the soluble intermediates at different stages during the microspheres formation were characterized by mass spectrometry. After reaction for 20 min at 180 °C in solvothermal conditions, no precipitation of the products was observed. The components of reactants/products solution were identified to be a mixture of **1**, mono- and disubstituted derivatives (Figure 4a and Figure S8 in the Supporting Information). These mono- or disubstituted derivatives should be involved in the substitution of 5, 10-positions of **1**, matching with the model reaction of **1** and **3** (mentioned above). After reaction for 60 min, the main component in the solution was disubstituted fluoranthene derivative **6** (Figure 4b), and the irregular spherelike solid products were seen at this stage (see Figure S9 in the Supporting Information). Longer reaction time did not yield any more extensively substituted species (e.g., triple- and tetra-substituted derivatives) in the solution but afforded more solid precipitation. Reacting for 24 h, however, the concentration of the disubstituted derivative in the solution was lower than the determination limitation of the mass spectrometry. Considering these experimental evidence, it is convincing that the formation of solid products is subject to the further reaction of the soluble disubstituted species **6**.

Starting from **6**, there are two pathways for the formation of solid precipitation: (1) **6** undergoes further sequential substitution with **2** to afford insoluble multisubstituted derivatives; (2) Cross-linking reactions among disubstituted species themselves create solid products. According to elemental analysis of produced

- (20) Crystal data for compound **4**: C₁₉H₃Cl₉N₂S₂, yellow, $M = 642.40$, triclinic, space group $P\bar{1}$, $a = 8.3193(7)$ Å, $b = 11.2070(8)$ Å, $c = 12.0009(9)$ Å, $V = 1086.75(14)$ Å³, $Z = 2$, $T = 173(2)$ K, $D_c = 1.963$ g cm⁻³, $\mu(\text{MoK}\alpha) = 1.367$ mm⁻¹, 9534 reflections collected, 4198 are independent ($R_{\text{int}} = 0.1071$). The final agreement factors are $R_1 = 0.0381$ ($I > 2\sigma(I)$) with 1891 data and $wR_2 = 0.0607$ for 4198 data based on 289 parameters.
- (21) Crystal data for compound **5**: C₂₅H₉Cl₇N₆S₆, yellow, $M = 833.89$, triclinic, space group $P\bar{1}$, $a = 11.8343(9)$ Å, $b = 12.3360(5)$ Å, $c = 12.7275(8)$ Å, $V = 1519.70(16)$ Å³, $Z = 2$, $T = 173(2)$ K, $D_c = 1.822$ g cm⁻³, $\mu(\text{MoK}\alpha) = 1.099$ mm⁻¹, 13118 reflections collected, 5226 are independent ($R_{\text{int}} = 0.0606$). The final agreement factors are $R_1 = 0.0727$ ($I > 2\sigma(I)$) with 2928 data and $wR_2 = 0.1853$ for 5226 data based on 397 parameters.
- (22) (a) Deng, S. L.; Xie, S. Y.; Lu, X.; Jiang, Y. B.; Fang, X. L.; Huang, R. B.; Zheng, L. S. *J. Mol. Struct.* **2007**, *829*, 51–56. (b) Deng, S. L.; Zhong, F. F.; Liang, H.; Huang, R. B.; Zheng, L. S. *J. Mol. Struct.* **2008**, *875*, 302–308.

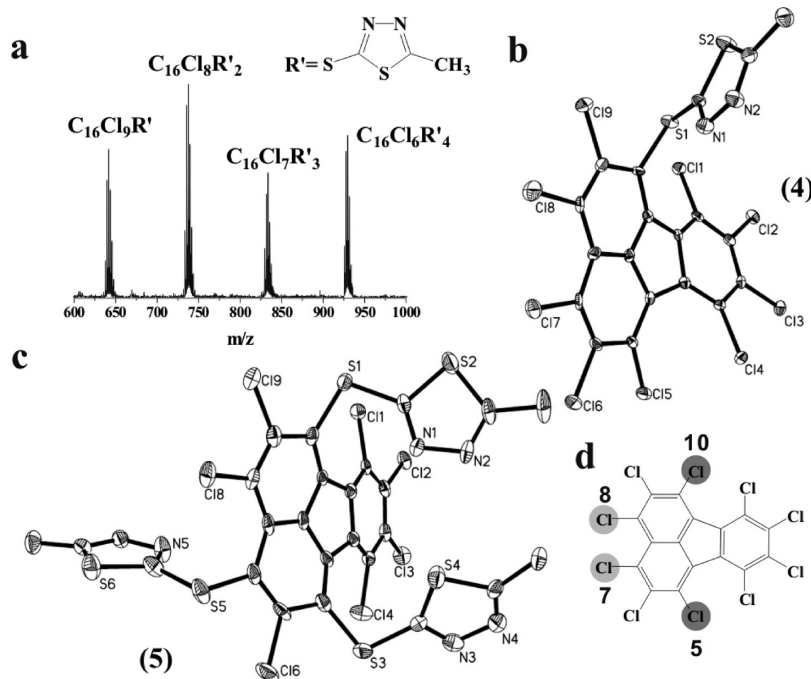


Figure 3. (a) Mass spectrum of the multisubstituted derivatives from the model reaction involving **1** with **3**. (b, c) Crystal structures of mono- and trisubstituted derivatives (compounds **4** and **5**) produced from the model reaction. (d) Schematic illustration of reactive sites in **1**; the dark gray circles are the most active chlorines, and the light gray circles are next most active ones.

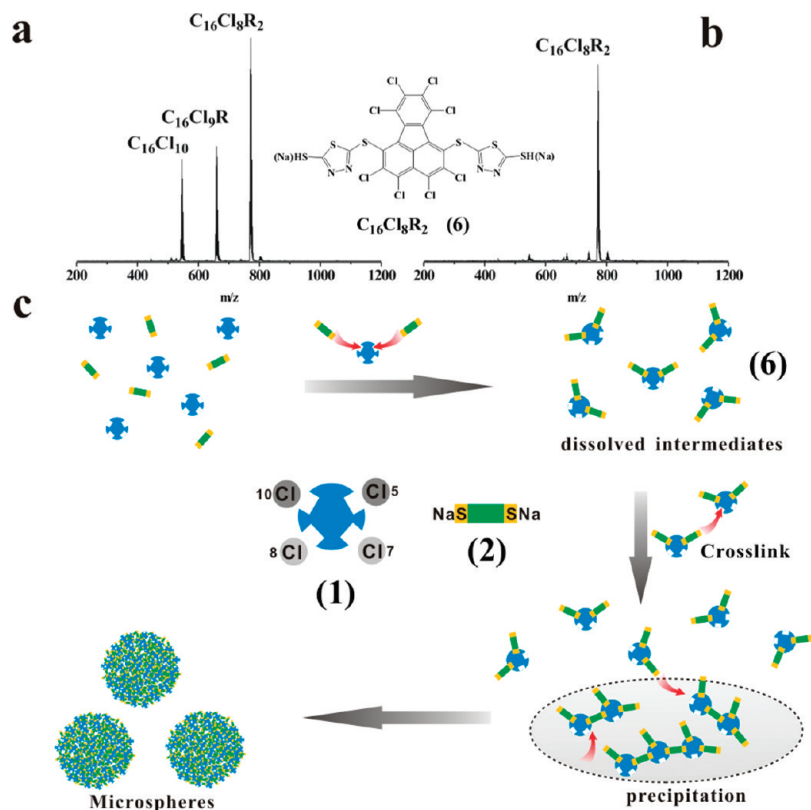


Figure 4. (a) Mass spectra of the reactants/products after reaction involving **1** with **2** for 20 min. (b) Mass spectra of the soluble components after reaction involving **1** with **2** for 60 min. (c) Schematic illustration of the possible cross-linking reaction involving disubstituted derivative **6**. The enlarged mass spectra of the mono- or the disubstituted derivatives are shown in Figure S8 in the Supporting Information.

fluorene-based microsphere materials (with 39.2% C and 32.0% S), the C/S ratio is about 1.23, which is approximately equal to the calculated results ($C/S = 1.25$) of **6**. Moreover, no other multisubstituted

derivative, e.g., tri- or tetrasubstituted ones, in the reaction solution during the microspheres growth was detected by mass spectrometry. It should be noted that tri- or tetrasubstituted derivatives would be readily detected

by mass spectrometry if they exist in the solution with concentration as low as the parts per million level, similar to the mass spectrometric analysis for the model reaction of **1** with **3** mentioned above. Therefore, we tentatively assume that the disubstituted derivative **6** is the main building block for construction of fluoranthene-based materials that are likely from the cross-linking reaction among disubstituted species themselves. Such a submission is not unreasonable because each molecule of **6** has four reactive groups, i.e., two $-SNa$ groups at 5,10-positions and two chlorine atoms at 7,8-positions of **1**. Accordingly, the reaction process for the fluoranthene-based solids can be schematically depicted in Figure 4c.

3.5. Routes for the Growth of Spherical and Tubular Morphologies. Although the fluoranthene-based microspheres and nanotubes have the similar chemical compositions, their aggregations with different shapes are controllable depending on the solvent conditions as depicted in Figure 1f. The major factor to influence their morphologies is associated with the solubility of organic solid reactant, i.e., perchlorinated fluoranthene **1**. For the growth of nanotubes, the optimal solvent is 1:32 toluene:methanol in which the reactant **1**, having crystalline nanorod morphology as shown in Figure 5, is hardly dissolved. Increasing the proportion of toluene in the mixed toluene/methanol solvent would decrease the nanotube yield but facilitate microsphere formation. At the 2:1 toluene:ethanol solution in which **1** can be completely dissolved, uniform microspheres dominate the products. On the basis of this experimental evidence, therefore, it is reasonable to speculate that the resultant morphologic alteration from microspheres to nanotubes is due to the change in initial shapes of the reactant **1** that is decided by the solvents used for the reaction. In other words, nanotubes grow from a nanorod-shaped solid of **1**, whereas microspheres form in a homogeneous solution of **1**.

To understand the growth process of the microspheres, a series of SEM images of the intermediates quenched during the microspheres growth were taken within the first 80 min of the reaction for morphological evolution (Figure 6). In addition to the typical self-assembly process involving nucleic formation and aggregation growth, the present case includes morphologies transformation from weblike to vesicle-like structures. At the first stage, the precipitation is formed as unshaped particles in nanometer scale. The reaction in the solution, with plenty of **1** and **2** as identified by mass spectrometry (vide supra), go on to precipitate onto the nanoparticles to form a weblike structure (Figure 6a). After reaction for 30 min, the weblike structures are destroyed and the precipitates turn to aggregate as bigger particles (Figure 6b). At this stage, there are plenty of disubstituted fluoranthene derivatives **6** in the solution, which has been assumed as the building block for the fluoranthene-based solids formation. At the reaction time around 35–40 min, vesicle-like structures are observed in the SEM images (Figure 6c, d). These vesicle-like structures have the sizes larger than the newly emerged nucleus, and facily encapsulate the nucleus interiorly. A typical TEM image of

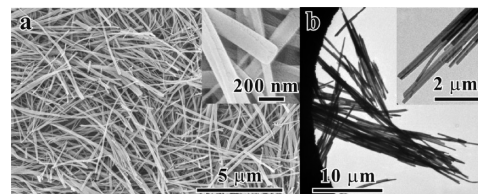


Figure 5. SEM (a) and TEM (b) images of the nanorod-shaped solids of **1** in toluene/ethanol (1:32) solution.

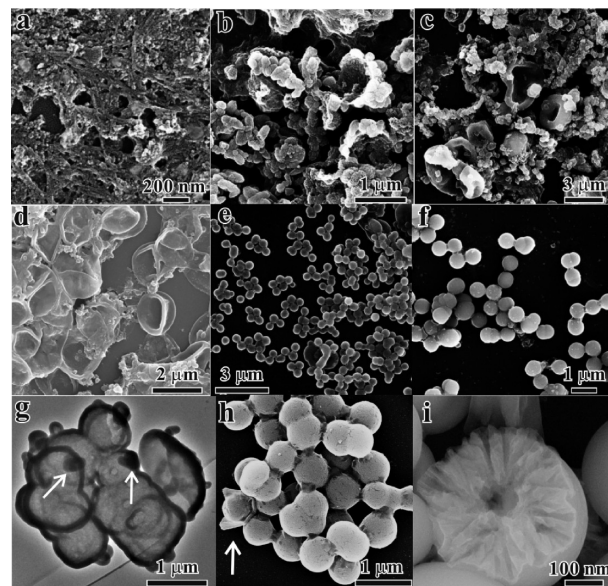


Figure 6. SEM images of the intermediates for the microspheres growth quenched at (a) 25, (b) 30, (c) 35, (d) 40, (e) 50, and (f) 80 min. (g) TEM image of the vesicle-like structures. (h, i) SEM images of the vesicle-like structures. All the intermediates were directly analyzed without any further treatment (e.g., washing by toluene/ethanol/water).

the vesicle-like intermediate structures is shown in Figure 6g, where some of the nucleus for microspheres growth are shown inside the vesicle-like structures (as the arrows pointing to). Via the nucleation mechanism in the vesicle surfaces, the spheres grow after reaction for 80 min (Figure 6c–f). During the aging period, the encapsulated spheres are wrapped by the vesicle shell in a sheet-folding mode. Figure 6i shows an unfinished sheetlike folding obviously, and more detailed information about the sheetlike shell wrapping the spherelike intermediates is shown in Figure S10 of the Supporting Information. The driving force of the total free enthalpy may be responsible for the morphology development, but further experimental or theoretical confirmation is required.

Different from microspheres growth, the formation of the fluoranthene-based nanotubes is involved in a template route. Convincing evidence to validate such submission comes from TEM images for the morphologic evolution of the intermediates/products quenched at different stages in the nanotube growth process. For better comparison, the captured intermediates samples were classified as two types for microscopic observation: one was direct observed by TEM without any cleaning treatment; another one was well-cleaned sequentially by toluene, ethanol and deionized water for SEM analysis. The intermediates obtained after reaction for 30 min were

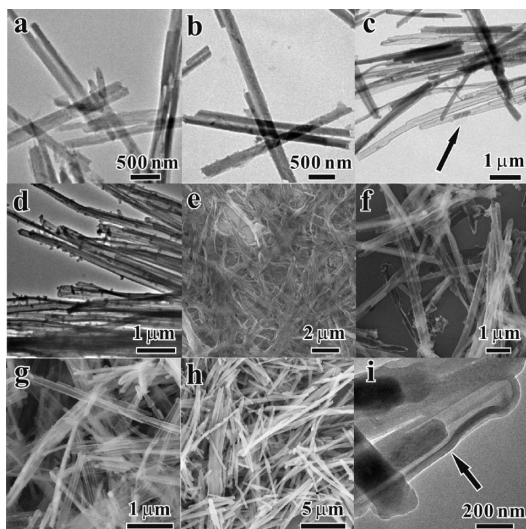
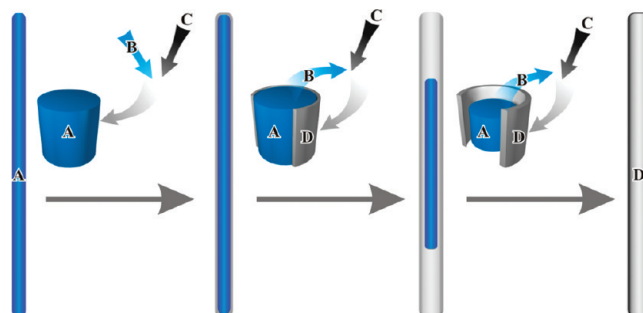


Figure 7. TEM and SEM images of the intermediates/products of the nanotubes quenched at: (a, e) 30, (b, f) 50, (c, g) 70, and (d, h) 24 h; (i) amplified TEM image of the typical intermediates.

solid nanorods with a diameter of about 200–400 nm (Figure 7a), but the nanorods were collapsed after treated by toluene (Figure 7e). Identified by mass spectrometry, the soluble component from these nanorods is perchlorinated fluoranthene itself (see the mass spectrum in Figure S11 of the Supporting Information). Similar results (Figure 7b) were observed in the products from the reaction for 50 min, but some of the products retained their one-dimensional morphology after washing with toluene (Figure 7f). The products trapped at 70 min were a mixture of nanotubes and nanorods (Figure 7c), and the intermediates of tubular structures with incompletely consumed core of **1** can be found in TEM (as the arrow pointing to). The tubular morphologies were remained after cleaning by toluene (Figure 7g), though **1** was still dissolved in toluene in a small quantities. After reaction for 24 h, almost all the products are featured with solid tubular structures, and no any signal of **1** was observed in mass spectrometric analysis of the toluene washing solution (Figure 7d, h). On the basis of the microscopic analyses, a growth route for the fluoranthene-based nanotubes is proposed as illustrated in Scheme 2: the nanorod of **1** serves as both template and reactant, and the produced sulfur-bridged fluoranthene deposited extensionally on the surface of the nanorod. With the consumption of **1**, the nanorod dissolves and extensionally deposited, leading to the narrow space between the interior fluoranthene solid (dissolving template) and the wall of the nanotube as shown in Figure 7i (an arrow pointing to). During such a template dissolving and extensionally depositing process, a series of intermediates featuring hollow fluoranthene-core/shell structures are frequently observed (see Figure S12 in the Supporting Information). Finally, the nanorods of **1** (i.e., the fluoranthene template) would completely convert to and deposit as the walls of the tubular structures. Under selected conditions, the inner diameter and length of the resultant nanotubes are well-consistent with those of the template (see Figure S13 in the Supporting Information).

Scheme 2. Schematic Illustration for Nanotube Growth^a



^aThe marks: A, template of **1** in the solid state; B, reactant **1** in the solution; C, reactant **2** in the solution; D, as-synthesized nanotubes.

This kind of template route is different from traditional methods for nanotubes growth, such as the sacrificial template method.²³ We nominate it as self-template synthesis. In principle, the self-template synthesis seems to be applicable to preparation of other organic nanomaterials with controllable morphology, if the solid reactants have defined morphology serving as the templates on which the products can be deposited.

On the basis of the proposed routes of self-assembly and self-template through the same Williamson reaction bridged with thioether group, indeed, we have been able to synthesize a series of microspheres and nanotubes starting from different arenes and sulfur-bridges. For example, the self-assembly of uniform arene-based microspheres has been achieved by the reaction between perchlorinated acenaphthylene and **2** (Figure 8a). The acenaphthylene-based nanotubes, similar to fluoranthene-based tubular structures, were also synthesized via the self-template process (Figure 8b). In addition, the synthesis of microspheres and nanotubes from Na₂S and **1** exemplifies that the sulfur-bridges can be altered to link the fluoranthene species (Figures 8c, d). These examples establish the versatility of the proposed methods for synthesis of various organic materials with desired morphologies.

3.6. Properties of the Fluoranthene-Based Organic Materials. In contrast to inorganic nanomaterials, the most prominent feature of the organic nanomaterials is the unavoidable organic groups remaining on their surfaces. These retained groups could be reactive like their parent organic molecules, leading to their reactivity higher than that of inorganic materials. Thanks to the incomplete consumption of thiol group in the cross-linking reaction during the fluoranthene-based materials growth, the thiol-containing organic micro/nano materials should have excellent chemical properties for further surface functionalization.²⁴

(23) (a) Steinhart, M.; Wehrspohn, R. B.; Gösele, U.; Wendorff, J. H. *Angew. Chem., Int. Ed.* **2004**, *43*, 1334–1344. (b) Mulvihill, M. J.; Rupert, B. L.; He, R. R.; Hochbaum, A.; Arnold, J.; Yang, P. D. *J. Am. Chem. Soc.* **2005**, *127*, 16040–16041.

(24) (a) Fan, Z. F. *Talanta* **2006**, *70*, 1164–1169. (b) Nakamura, M.; Ishimura, K. *Langmuir* **2008**, *24*, 5099–5108. (c) Kim, S. W.; Kim, M.; Lee, W. Y.; Hyeon, T. *J. Am. Chem. Soc.* **2002**, *124*, 7642–7643. (d) Yi, D. K.; Lee, S. S.; Ying, J. Y. *Chem. Mater.* **2006**, *18*, 2359–2461. (e) Gao, F.; Lu, Q. Y.; Zhao, D. Y. *Chem. Phys. Lett.* **2002**, *360*, 585–591.

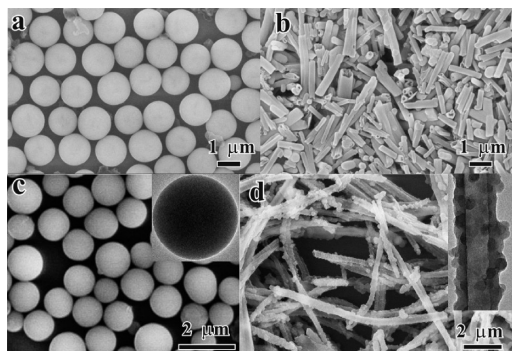


Figure 8. SEM images of the acenaphthylene-based (a) microspheres and (b) nanotubes synthesized from perchlorinated acenaphthylene. SEM/TEM images of the fluoranthene-based (c) microspheres and (d) nanotubes obtained from the reaction involving $\text{Na}_2\text{S}\cdot 9\text{H}_2\text{O}$ and **I**.

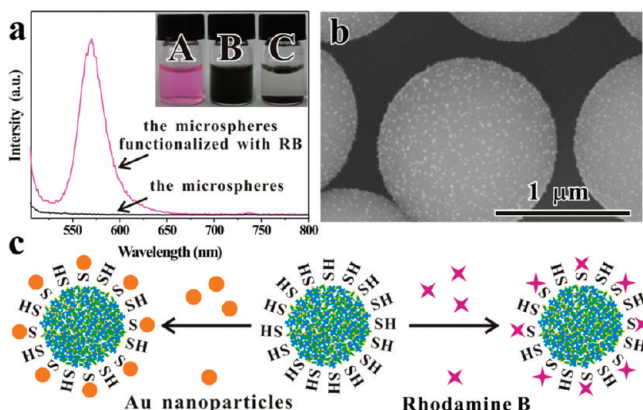


Figure 9. (a) Emission spectra of the RB functionalized microspheres and the pristine microspheres dispersed in water. The inset shows (A) the suspension/solution colors of RB solution, (B) the mixture of microspheres with RB solution before the functionalization reaction, and (C) the RB functionalized microspheres precipitation after the functionalization reaction. (b) Typical SEM image of the as-synthesized microspheres coated with Au nanoparticles. (c) Schematic illustration of the surface functionalizations.

Taking the synthesized microspheres as an example, the thiol groups retained on the surface can readily react with the carboxyl groups of Rhodamine B (RB) to functionalize the organic microspheres as fluorescent materials.²⁵ As shown in the inset of Figure 9a, after reacting with the microspheres for 15 min, the color of RB solution changed from pink to colorless. Although the originally pristine microspheres do not show the luminescence of the chromophores, the resultant RB-functional microspheres emit around 570 nm, the characteristic wavelengths of RB. The evidence implies a promising application of the microspheres functionalized as fluorescent materials.²⁴

In addition, these thiol-containing micro/nano materials are also applicable for preparation of functional materials coating with noble metals or metal sulfide nanoparticles.²⁴ For example, Au nanoparticles can be attached to the microspheres in the solution of $\text{HAuCl}_4/\text{sodium citrate/sodium borohydride}$. Figure 9b shows the typical SEM image of the Au-coating microspheres with gold nanoparticles of about 20 nm. These well-dispersed

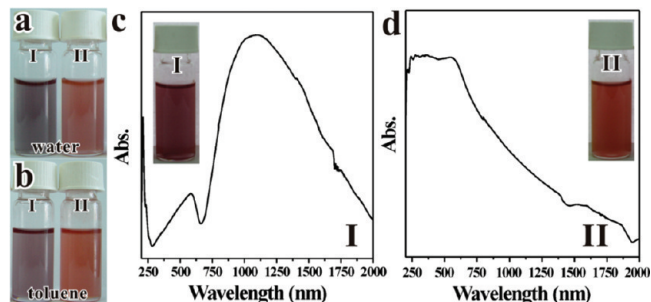


Figure 10. (a, b) Photos of the as-synthesized (I) microspheres and (II) nanotubes dispersed in (a) water and (b) toluene, respectively; (c, d) UV-vis-NIR spectra of the (c) as-synthesized microspheres and (d) nanotubes dispersed in ethanol; the insets are the corresponding photos.

Au-functionalized microspheres can be useful for catalyst applications.²⁶

The chemical groups remaining on the surfaces of the organic nanomaterials also define the dispersion of organic substances in polar and nonpolar solvents. Due to the coexistence of thiol- and aromatic-moiety, the synthesized fluoranthene-based materials may be dispersed well in both polar and nonpolar solvents. Indeed, in contrast to most inorganic nanomaterials that usually aggregate in organic solvents because of the hydrophobic groups on their surfaces, the synthesized organic materials can be well-dispersed in water or toluene to show their biphilic properties (Figure 10a,b).

Remarkably, the optical properties can be tuned depending on the morphologies of the fluoranthene-based materials. As shown in the insert of Figure 10c, d, taking the reactant **I** and the as-synthesized microspheres/nanotubes into consideration, their colors of dilute suspensions in ethanol are obviously different. Figure 10c,d shows the UV-vis-NIR absorption of the fluoranthene-based microspheres and nanotubes recorded in ethanol solution, respectively. Interestingly, although the microspheres and the nanotubes have the similar chemical composition, NIR absorption ranging from 700 to 2000 nm is observed only in the microspheres (with a absorption coefficient of $5.71 \text{ L g}^{-1} \text{ cm}^{-1}$, see Figure S14 in the Supporting Information). Although the absorption bands in the region from 300 to 700 nm can be attributed to $\pi-\pi^*$ and $n-\pi^*$ transitions of the conjugated aromatic,²⁷ the absorption bands in the region from 700 to 1800 nm imply an extended conjugation length and an enhanced intramolecular charge transfer in the microspheres. We rule out the possibility of the NIR signals producing from the scattering of microspheres through a contrastive trial with inorganic microspheres of comparable size, and tentatively assume the unique self-assembly via a vesicle route to form encapsulated spheres enwrapped by the vesicle shell in a sheet-folding structure may contribute to the enhanced NIR absorption. Although the broad NIR absorption implies a complex mechanism, the

(26) Ge, J. P.; Huynh, T.; Hu, Y. X.; Yin, Y. D. *Nano Lett.* **2008**, *8*, 931–934.

(27) (a) Ajayaghosh, A. *Acc. Chem. Res.* **2005**, *38*, 449–459. (b) Small, D.; Zaitsev, V.; Jung, Y. S.; Rosokha, S. V.; Head-Gordon, M.; Kochi, J. K. *J. Am. Chem. Soc.* **2004**, *126*, 13850–13858.

(25) Howard, A. G.; Khadry, N. H. *Analyst* **2004**, *129*, 860–863.

morphology-dependent properties of the fluoranthene-based materials have been unambiguously shown.

4. Conclusion

In summary, we have developed a novel and simple method for controllable synthesis of the thiadiazole-containing sulfur-bridged fluoranthene-based microspheres and nanotubes. Morphologies of the products are controllably subjected to the original shaped of reactants that are defined by the solubility of the reactant in the solvent mixture of the reaction system. Identified by mass spectrometry, X-ray photoelectron spectroscopy and crystallography, a disubstituted derivative of perchlorinated fluoranthene has been established as the basic building units for the solid products. By trapping the intermediates during the fluoranthene-based materials growth, a self-assembly and a self-template route are proposed for understanding the formation of the microspheres and the nanotubes, respectively. The proposed methods are versatile for construction of other arene-based molecular materials with desired morphologies. One of the most prominent properties of the as-synthesized materials is the chemical reactivity involving the thiol groups retained

on the surface of the molecular microspheres or nanotubes. Such a chemical reactivity makes them valuable for further synthesizing functional materials coupled with metals or fluorescent groups for potentially technological applications. A strong absorption is observed for the microspheres in the wavelength range of 700–1800 nm, whereas there is a silent absorption for the nanotubes in this NIR range. Such a NIR absorption difference proves the morphology-dependent properties of the fluoranthene-based materials. The synthesis, mechanism, and potential applications of the fluoranthene-based materials reported in this contribution mark the beginning of investigation on a novel class of promising functionalized organic molecular materials.

Acknowledgment. This work was supported by the National Natural Science Foundation of China (Grant 20525103, 20721001, and 20531050) and the 973 Program (Grant 2007CB815301).

Supporting Information Available: Figures S1–S14, Table S1 (PDF). The crystallographic information files of compound **4** and **5** (CIF). This material is available free of charge via the Internet at <http://pubs.acs.org>.